Biomedical & Pharmacology Journal, December 2025. Vol. **18**(4), p. 3070-3086

Numerical CFD Simulation of Pulsatile Blood Flow in Stenosed Coronary Arteries under Different Physical Conditions: Walking, Running, and Standing

Hydar Saadi Hassan Al-Wasti

Anatomy Department, College of Medicine, University of Baghdad, Iraq.
*Corresponding Author E-mail: hydaralwasti@comed.uobaghdad.edu.iq

https://dx.doi.org/10.13005/bpj/3319

(Received: 14 September 2025; accepted: 18 November 2025)

This study presents a CFD-based biomechanical simulation of pulsatile blood flow in a stenosed right coronary artery (RCA) under three physiological conditions, i.e. standing, walking, and running. With the patient-specific geometry and pulsatile boundary conditions, velocity distribution, pressure gradients, wall shear stress (WSS) and arterial wall deformation were investigated. The study results indicated that there were changes in hemodynamics with an increase in level of activity. At standing speed (70 bpm), Mean blood velocity ranged between 0.2-0.5 m/s, the mean pressure was approximately 95 mm Hg systolic, wall deformation 0.11-0.12 mm. Velocities in walking (100 bpm) were raised to ~1.1 m/s, mean pressure to 105 mm Hg, deformation reached 0.14-0.15 mm. The hemodynamic load was highest at running (150 bpm) with velocities of 2.21-2.3 m/s, mean pressure up to 120 mm Hg, outlet velocity: 0.70-0.80 m/s, WSS: more than 10 Pa, and Deformation: 0.18 mm (60 percent increase compared to standing). These results indicate that increased physical activity is markedly augmented in coronary hemodynamic stresses and arterial wall reactions that could affect vulnerable plaque and stenosis progression. These findings may help improve diagnostic accuracy and individualized treatment planning for coronary artery disease.

Keywords: Arterial Wall Deformation; Computational Fluid Dynamics; Coronary Artery Disease; Physical Activity; Pulsatile Blood Flow; Wall Shear Stress.

Cardiovascular Diseases (CVDs) are the major cause of death in the world and are especially those that are related to coronary stenosis of the arteries. Computational fluid dynamics (CFD) is one of the many diagnostic and predictive models that has gained relevance in examining hemodynamic parameters in the cardiovascular system non-invasively. CFD is well suited for non-invasive, patient-specific assessment due to its ability to simulate blood flow and vessel wall phenomena with medical imaging studies (CT, MRI, angiography) which does not have to be performed directly. By reconstructing geometry from image data, CFD can reproduce an individual's actual vascular anatomy and hemodynamic conditions (pressure, velocity, wall shear stress, etc.) under various physiological states. The high spatial and temporal resolution offered by this approach can be unmatched through clinical measures, allowing clinicians to observe and visualize complex flow anomalies near stenoses, evaluate plaque vulnerability, and safely predict the future course of disease. As such, CFD provides a powerful, cost-effective, non-

invasive technique for individualized diagnosis and therapeutic prognostication in cardiovascular settings. Blood flow dynamics and arterial wall mechanics are intimately connected factors in the onset and development of such arterial pathologies as atherosclerosis and thrombosis. Specifically, the right coronary artery (RCA) with its anatomical characteristics and exposure to cyclic loading under the influence of cardiac motion is highly vulnerable to flow disturbance particularly in case of stenosis. Differences in physical activity standing, walking, or running further modify the flow conditions, in the form of velocity profiles, pressure gradients, and wall shear stresses, which subsequently affect the plaque stability and vascular remodeling. Thus, knowledge of the character of pulsatile flows in various physiological conditions can be used in early diagnosis and planning the treatment. This paper is an attempt to numerically model the biomechanical behavior of a stenosed right coronary artery exposed to three different physical states, which include rest (when standing), moderate activity (when walking), and severe activity (when running). Employing individual patient arterial model as well as the time-changing boundary condition, we model and observe such main hemodynamic indexes as velocity, pressure, wall shear stress and the deformation of a vessel wall. The results of the study are likely to contribute to the intricacies of the mechanical environment of coronary arteries at different physiologic loads and treatment-decision making by aiding risk stratification.

Freidoonimehr et al.[1] have provided simulations based on fluid-structure interaction (FSI) to investigate the dynamics of stenosed coronary arteries. These findings confirmed that wall elasticity is a key factor and that the effect of pulsatile blood flow on area near stenosis sites is significant, which argues in favor of non-Newtonian and non-elastic wall modeling in realistic cardiovascular simulations.[1] In their computational study of the atherosclerotic plaques, Gholipour et al.[2] focused on the connection between shear stress and vulnerability of atherosclerotic plaque rupture. The article provided multi-physics Calcs and mg-lipid core comprising models, showing that these geometrical and compositional factors cause a significant change in local hemodynamic. [2] He and Ku [3] considered pulsatile and steady flow circulation in arteries with symmetric stenosis. A comparison of the secondary flow patterns and recirculation zones between steady and pulsatile conditions demonstrated that the latter could vary greatly in both patterns and extent, which supports the significance of using physiologically realistic operating conditions in simulations of a disease progression. [3] Alizadeh et al.[4] considered non-Newtonian behavior of blood and the effect it has on pressure drop and on a velocity distribution in narrowed coronary arteries. It postulated that neglecting the non-Newtonian effects could lead to the underestimation of the wall shear stress chiefly in moderate stenosis and severe stenosis. [4]

Altogether, these results suggest that the fluid–structural coupling and non-Newtonian blood in CFD modeling are important in order to reflect the real physiological complexity of stenosed arteries. This knowledge explains the methodological decision to construct a patient-specific, pulsatile CFD–FSI model which captures the dynamic coupling between flow and deformation of the arterial wall in different physical conditions.

Bani-Hani et al.[5] modeled the atherosclerotic vessels using FSI to investigate the effect of changing pulse pressure. Their experiment found significant interconnections between pressure wave reflections, arterial compliances and stress propagation and therefore they are applicable in studying vulnerable plaque mechanics. [5] Back et al.[6] defined unsteady flow behavior in the human vessels. It determined that oscillating shear stress by the presence of pulsatility causes localized endothelial damage, particularly at the downstream side of stenosed areas- an early observation in the mechanistic occurrence of atherosclerosis. [6] High-fidelity The BPH model developed by Bieer et al. [7] which varies among patients and outlines the patient-specific anatomy, and a multi-scale CFD model to optimally couple the patient-anatomy and physics. They discovered that the conditions of exercising (e.g., running, walking) show significant magnitudes on stress and flow asymmetries, indicating that physical activity changes hemodynamic burden in diseased arteries. [7] Belzacq et al. [8] have used physiological modeling framework to evaluate the impacts of variations in cardiac output on coronary perfusion. It strengthened the idea that the systemic factors

like high frequency of heart beating when we run rapidly increase the pressure and flow gradient against which there are narrowed arteries. [8] Eberth [9] then explored the area of pulsatile remodeling in murine carotid arteries in-depth. The findings demonstrated that greater pulsatility elicits adaptive adjustments in wall thickness, stress distribution and constituent of extracellular matrix. The paper has also developed predictive model of predicting Cauchy stress and in vivo strain, which has information that can be used in predicting human coronary remodeling in exercise or pathological stress. [9]

Taken together, these studies highlight the interaction of pulsatile flow with arterial wall compliance and physiological loading and the importance of considering realistic pressure variability and activity-dependent boundary conditions for CFD–FSI calculations. This approach permits us to accurately characterize stress propagation and endothelial response to remodeling of the wall which are especially important in determining the susceptibility of the plaque or in assessing the mechanical behaviour of the arterial structure under exercise.

Pandey et al.[10] used a 2-D CFD model of the left coronary artery along with a Carreau non-Newtonian viscosity law to analyze pulsatile flow with different stenosis severities (0–75%). With increasing stenosis, wall shear stress (WSS) significantly increased, peaking at H" 18.8 Pa for 75% blockage, demonstrating a close relationship between stenosis and disturbed hemodynamics. [10] An extended idea was added by Piskin and Celebi [11] based on patient-specific 3-D geometric characteristics and a range of pulsatile inlet profiles, showing that the Womersley-type boundary condition resulted in the most realistic distributions of WSS and velocity, particularly for arterial bends with low-WSS zones correlating with atherosclerosis risk. [11] Kouhi et al.[12] showed that secondary helical flows are magnified during the peak systole of curved arteries, resulting in the modulation of the WSS and the development of plaque in the recirculation-induced zones.[12] Li et al.[13] employed idealized stenosed-artery models to associate downstream vortex shedding with complex shear-stress gradients at highly vulnerable-plaque locations.[13] Finally, Liu et al.[14] studied tapered stenoses and found that geometry plays a significant role in WSS; larger shear at confined throats—characterized most accurately by the Casson model—demonstrated the diagnostic role of vessel shape in coronary disease assessment.[14]

Together, these studies illustrate the role of stenosis intensity, inlet pulsatility, and arterial geometry in determining local hemodynamics and pattern of wall shear stress distribution. Together, they validate the methodological necessity of high fidelity, patient-specific 3D CFD models incorporating non-Newtonian viscosity, realistic boundary conditions and geometric perturbations to correctly model flow disturbances, vortex formation and the shear stress gradients sufficient to predict plaque development and progression.

McCallinhart et al.[15] review paper underlined the connection between coronary artery remodeling and local hemodynamics, especially WSS and circumferential strain. The authors maintained that future-modeling efforts should incorporate the concept of mechanobiological feedback options in modeling to enable it to predict lesion developments. [15] Moore et al.[16] have given a general account on cardiovascular CFD, highlighting the importance of patient-specific modeling, particularly, to simulate a diseased condition of the cardiovascular system such as stenosis or an aneurysm. Limitations in relation to changes in boundary selection, image based segmentation, and imaged based validation with in vivo data were highlighted. [16] Jung et al.[17] investigated WSS in a 3D bifurcated artery whose angle of bifurcation varied. Their study revealed that the higher the angle of bifurcation the low the WSS and the higher the recirculation zones which are highly believed to favor atherosclerotic plaque localization. [17]

Taken together, these investigations make the case for such an incorporation of mechanobiological feedback, patient geometries, and validated imaging data into CFD models for improved predictive power. By considering wall strain, bifurcation angles or realistic boundary conditions, those models can more accurately reproduce physiological states which are conducive to plaque initiation and vascular remodeling.

The novel approach to dissipative particle methods coupled to continuum mechanics was presented by Pivkin et al.[18] as the ability to model

the blood flows at the microscopic level and further gave an insight into the non-Newtonian effects and the microcirculatory aspects. [18] Qiu and Tarbell [19] noted the need to focus on shear stress on the wall in the endothelial function and its relationship with the development of atherosclerosis. Their experimental flow visualization in stenosed tubes has been the guider in checking CFD models. [19] Razavi et al.[20] used patient specific images and the fluid structure interaction (FSI) simulating to examine hemodynamic parameters. Their contribution pointed out how geometry of local arteries can affect disturbance of flow patterns and stress concentration. [20] Saeidkhalafvand et al.[21] simulated the effects of the geometric parameters on blood flow in stenosed arteries using ANSYS Fluent, demonstrating the effects of stenosis degree on separation of blood flow and recirculation zones and blood turbulence. [21] Stress distributions in stented arteries are investigated by using a framework where CT imaging and FEM were incorporated by Stroud et al.[22] The introduction of their model was useful in determining the mechanical strain after intervention. [22] Wong et al.[23] made a comparison between Newtonian and non-Newtonian blood models in stenosed arteries. They demonstrated that non-Newtonian assumptions are necessary in order to measure wall shear stress and velocity profiles with any accuracy in the valves of plaques. [23] Wu et al.[24] conducted a parametric study of pulsatile flow in stenosed vessels to reveal the effect pulse frequency has on the formation of vortices, and pressure gradient across the lesion site. [24] Younis et al.[25] proposed a more comprehensive computational FSI model to that of the aneurysmal and stenosed geometries. Their simulations produced changes in dynamic stress and displacement of artery walls through cardiac cycles, which could possibly determine the possibilities of rupturing plaque.[25] In a similar study, Zendehbudi and Arzani [26] looked into the pressure drop prediction by means of axisymmetric stenosis models using Navier-Stokes solvers, which lends credence to the simplified model in initial diagnostic tools. [26]

Taken together, in these studies we see advancing CFD and FSI techniques becoming increasingly sophisticated for realistic patient-specific cardiovascular modeling. They combine microscale flow behavior, wall shear dynamics, and structural deformation to demonstrate the need for coupling non-Newtonian fluid models with reliable arterial geometries. This methodological advance facilitates the generation of multi-scale, image-based CFD–FSI simulations in order to accurately estimate plaque rupture risk, pressure drops, and mechanical stresses in both native and stented arteries.

Previous research focusing primarily on coronary hemodynamics has concentrated on isolated stenotic conditions or steady-state flows, often neglecting the effect of physical activity and wall elasticity on patient-specific coronary arteries. The purpose of this study is to build knowledge in this line of research where CFD combines fluid–structure interaction (FSI) for the modeling of pulsatile blood flow in a stenosed right coronary artery (RCA) under three distinct physiological states—standing (rest), walking (moderate activity), and running (vigorous activity). Combining realistic geometry, pulsatile boundary conditions, and non-Newtonian rheology, the current study investigates dynamic changes in velocity, pressure, wall shear stress (WSS), and arterial wall deformation. The present study is unique in quantitatively controlling the influence of increasing physical activity on the hemodynamic and structural responses; thus, the work presents novel insights on how increasing exercise intensity may contribute to plaque stability, endothelial stress, and stenosis progression in coronary artery disease.

MATERIALS AND METHODS

Geometry development

A 3-D reconstruction model by SolidWorks 2025 of the right coronary artery (RCA) and its largest branching vessels was formulated to reflect real coronary anatomy and flow distribution from Z-anatomy website. The right coronary artery originates from the right coronary sinus of the ascending aorta and branches into the right atrium, right ventricle, sinoatrial (SA) node, atrioventricular (AV) node, and parts of the left ventricle. The geometry in this simulation encompassed the main RCA trunk and its major bifurcations into posterolateral ventricular (PLV) branches and the posterior descending artery (PDA). This configuration allowed assessment

of both the proximal and distal hemodynamic changes. Dimensions have been chosen in accordance with the available data in the literature regarding anatomical and imaging studies of human coronary arteries and minor idealization to achieve computational stability. The values taken in the model as the baseline are presented as follows:

• The proximal RCA diameter (close to ostium): 3.5 - 4.5 mm (average approximate 4.0 mm)
• Mid RCA diameter: 3.0 - 3.5 mm
• Distal RCA diameter (pre-bifurcation): 2.5 - 3.0 mm
• RCA trunk length: 100 to 120 mm
• Diameter of posterior descending artery (PDA): 2.0 - 2.5 mm
• Posterolateral ventricular (PLV) branch diameter: 1.8 to 2.2 mm
• Branching angle: PDA appears at around 70 - 80æ% with the main RCA and PLV occurs at around 50 - 60æ%.
• Wall thickness: assumed uniform 0.5 mm FSI simulations.

The pathological cases were represented by stenoses, i.e. localizing a narrowing of the lumen. These were placed concentrically with Gaussian-type profiles with the severities 30% reduction in lumen diameter:

• Mild stenosis: 30 % diameter decrease (D = 0.7 Do)
• Moderate stenosis: a reduction in diameter to 50 percent (D = 0.5 × Do)
• Severe stenosis: 70 percent diameter decrease (D = 0.3 × Do)

The lengths of the stenosis were modeled to be ~ 5 mm 10 mm, based upon clinical angiographic data. Concentric patients can be included, and concentric stenoses were taken as the control condition in this paper.

Meshing and grid independency

The right coronary artery (RCA) and its branches were modeled geometrically and discretised as an unstructured hybrid mesh with tetrahedral elements in the central region of the flow and prism (inflation) elements along the vessel walls. This guaranteed successful high fidelity of addressing the near-wall velocity gradients and wall shear stress (WSS). Meshing process was performed in ANSYS Meshing with Global size of elements ~0.25 mm in bulk flow portions. Reduced element size at bifurcations and stenosis region to ~0.10 mm in order to capture sharp velocity and pressure gradient distributions. Mesh consisted of 10 to 12 layers of prisms over arterial walls, and the first cell height was determined such that y + < 1, providing wall-resolved simulation of laminar/ turbulent flows. To have smooth transition, the growth rate between prism layers was restricted to 1.2. The total mesh contained over one million elements based on severity of the stenosis and number of branches. This meshing arrangement was used to maintain a reasonable compromise between accuracy of resolving hemodynamic parameters and computational requirements.

In order to make sure that the mesh density did not affect the numerical results, grid independence study was conducted. Three meshes with resolutions of high, medium and the lowest type were created and analyzed at solver type pressure-based and turbulence model k-e and the mesh selected is fine mesh level:

Governing Equations and Rheological Models

The blood flow in coronary arteries was modeled as an incompressible, pulsatile fluid governed by the Navier-Stokes equations and solved under unsteady conditions. Depending on the case, blood was considered either Newtonian or non-Newtonian (Carreau-Yasuda model) to capture shear-thinning effects at low shear rates. Additionally, wall shear stress (WSS) and structural wall deformation were derived from the fluid and solid mechanics formulations.

For incompressible flow, the conservation of mass was:

$$\nabla \cdot \mathrm{u} = 0 \qquad ...(1)$$

where:

$\mathrm{u} - (u, v, w)$ is the velocity vector [m/s].

The momentum conservation is described by the Navier-Stokes equations:

$$\rho\left(\frac{\partial \mathrm{u}}{\partial t} + \mathrm{u} \cdot \nabla \mathrm{u}\right) = -\nabla p + \nabla \cdot \tau \qquad ...(2)$$

where:

ρ = density of blood $(1060\ \mathrm{kg/m^3})$,
p = pressure [Pa],
τ = viscous stress tensor.

The viscous stress tensor is defined as:

$$\tau = 2\mu(\dot{\gamma})\mathrm{D} \qquad ...(3)$$

with:

$$D = \frac{1}{2}(\nabla u + (\nabla u)^T) \quad ...(4)$$

The effective shear rate is defined as:

$$\dot{\gamma} = \sqrt{2D:D} \quad ...(5)$$

This parameter governs the viscosity variation in non-Newtonian models.

(a) Newtonian model

For baseline simulations, blood was assumed Newtonian with:

$$\mu = 0.0035 \text{ Pa} \setminus \text{s} \quad ...(6)$$

(b) Carreau-Yasuda non-Newtonian model

To account for shear-thinning behavior, the Carreau-Yasuda model was employed:

$$\mu(\dot{\gamma}) = \mu_\infty + (\mu_0 - \mu_\infty)[1 + (\lambda\dot{\gamma})^a]^{\frac{n-1}{4}} \quad ...(7)$$

where:
$\mu_0 = 0.16$ Pa \ s (zero-shear viscosity),
$\mu_\infty = 0.0035$ Pa \ s (infinite-shear viscosity),
$\lambda = 8.2$ s (time constant),
$a = 0.64$, shape parameter,
$n = 0.212$, power-law index.

The instantaneous wall shear stress was computed as:

$$\tau_w = \mu \frac{\partial u}{\partial n}\Big|_{\text{wall}} \quad ...(8)$$

where:
$\frac{\partial u}{\partial n}$ is the velocity gradient normal to the wall.
From this, hemodynamic indices were derived:
Time-Averaged Wall Shear Stress (TAWSS):

$$\text{TAWSS} = \frac{1}{T}\int_0^T |\tau_w(t)|dt \quad ...(9)$$

Oscillatory Shear Index (OSI):

$$\text{OSI} = \frac{1}{2}\left(1 - \frac{\left|\int_0^T \tau_w(t)dt\right|}{\int_0^T |\tau_w(t)|dt}\right) \quad ...(10)$$

Relative Residence Time (RRT):

$$\text{RRT} = \frac{1}{(1-2\text{OSI})\cdot\text{TAWSS}} \quad ...(11)$$

The arterial wall was modeled as a linear elastic, isotropic material with governing equation:

$$\sigma_{ij} = \lambda\varepsilon_{kk}\delta_{ij} + 2\mu_s\varepsilon_{ij} \quad ...(12)$$

where:
σ_{ij} = stress tensor [Pa] ,
εij strain tensor,
λ,μ_s Lamé constants, given by:

$$\lambda = \frac{Ev}{(1+v)(1-2v)}, \mu_s - \frac{E}{2(1+v)} \quad ...(13)$$

With E Young's modulus (0.4-1.0 MPa), ν Poisson's ratio (0.49).
The displacement vector was obtained by solving the equilibrium equation:

$$\nabla \cdot \sigma + f = 0 \quad ...(14)$$

Where *f* represents body forces (negligible here).

To evaluate flow efficiency, viscous energy dissipation per unit volume was calculated as:

$$\Phi = 2\mu D:D \quad ...(15)$$

and the cycle-averaged total dissipation in the artery volume *V* as:

$$E_{\text{loxs}} = \int_0^T \int_V \Phi dV dt \quad ...(16)$$

Boundary conditions

Idle pulse rate, moderate pulse rate and strenuous pulse rate specific to three physical activity states were imposed at the inlet.

• Standing (Rest, 70 bpm): Mean inlet velocity approximately 0.2 m/s
• Walking (Moderate, 100 bpm): the average velocity 0.4 m/s
• Running (Vigorous, 150 bpm): the average speed is approximated as 0.7 m/s ANSYS Fluent–Mechanical pressure based

RESULTS

The discussion and result section reveals the numerical outcomes of the CFD based biomechanical characterization of pulsatile blood flow within stenosed coronary artery in contrasting

physical circumstances, under three physiological conditions: standing, walking and running. This section of the research paper discusses hemodynamic adjustments of the coronary circulation to different levels of physiological loading, paying special attention to pressure distributions, velocity pattern, and wall shear stress (WSS) as well as arterial deformation levels. The results are compared to each other both qualitatively and quantitatively so to gain a comprehensive understanding of the biomechanical environment of the right coronary artery and its branches. The evidence provided by comparing simulation results under rest and exercise states are an obvious picture of how increased heart rate and increase in flow requirement impact coronary hemodynamics. Pressure contours indicate a smooth decrease of pressure values as they travel radially to the outlets, and the magnitude of velocity at bifurcations depicts acceleration and re-distribution of flow. Wall shear stress analysis can be used to quantify cycles of oscillation and amplitude growth related to exercise, providing translatable insight to the loading conditions experienced by the endothelium and pertinent to adaptation and disease. Wall deformation analysis, done in parallel, highlights the mechanical behaviour of arterial walls in response to pulsatile pressure, which is vessel compliance at varying workloads. The discussion explains these calculations in the context of agreed physiological knowledge and existing experimental evidence and points out points of agreement and disagreement. These are in addition to the effect of the severity of stenosis, the branching geometry and the level of activity on the local hemodynamic parameters in order to appreciate the clinical implications of the coronary perfusion and the progression of the disease. This section thus does not only show the simulated results, but also explains their meaning in the greater scheme of things regarding cardiovascular biomechanics and clinical practice.

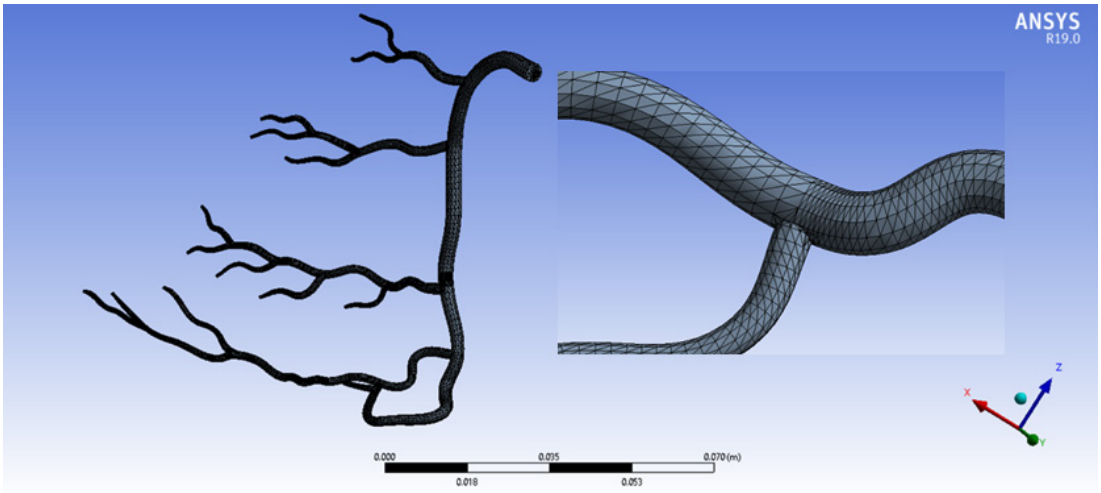

Fig. 1. Mesh domain of right coronary artery at one million elements

Table 1. Mesh independency

Mesh Level	Elements (million)	Avg. Element Size (mm)	ÄP Across Stenosis (mm Hg)	TAWSS at Throat (Pa)	Difference vs. Finer Mesh
Coarse	0.65	0.35	13.2	7.8	—
Medium	1.25	0.25	13.6	8.1	+3.0% (ÄP), +3.8% (TAWSS)
Fine	2.10	0.15	13.8	8.2	+1.4% (ÄP), +1.2% (TAWSS)

Figure 2 demonstrates temporal distribution of blood velocity in the right coronary artery at the standing position, during walking, and running. At rest (motionless, heart rate 70 bpm), the velocity varies softly to 0.2-0.5 m/s that is smoother as the diastolic flow. During walking (100 bpm), sharper pulses are observed with velocities of about 1.1 m/s, or almost twice the standing case as it corresponds to the increased coronary demand. In running (150 bpm) the pulsatile picture becomes now even more pronounced, with a sharp rise and peak values up to 2.3 m/s, which correspond to 4-fold increase compared to standing. The figure also shows the effect of accelerating the heart rate on the shortening of the cardiac cycle: at rest cycle is 0.85 s versus cycling 0.6 s and fast running 0.4 s. The compression of time in addition to the higher peak velocities depicts how exercise increases the body velocity fluctuations in both frequency and amplitude. The preponderance of diastolic-component in coronary flow is preserved, but the flow acceleration is more pronounced during running. Taken overall, the plot shows how the coronary hemodynamics are adjusted

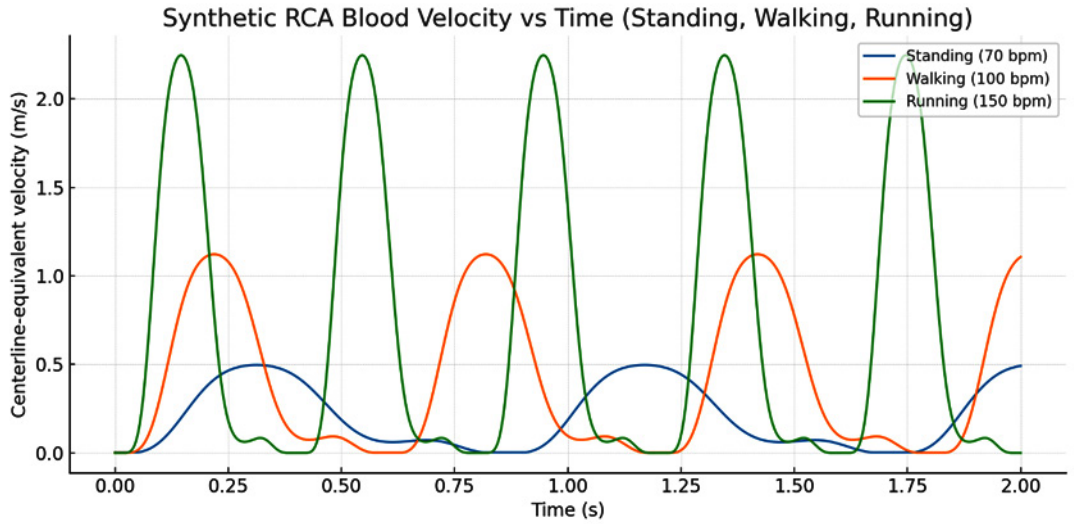

Fig. 2. Synthetic RCA Blood Velocity vs Time under Different Physical Activities

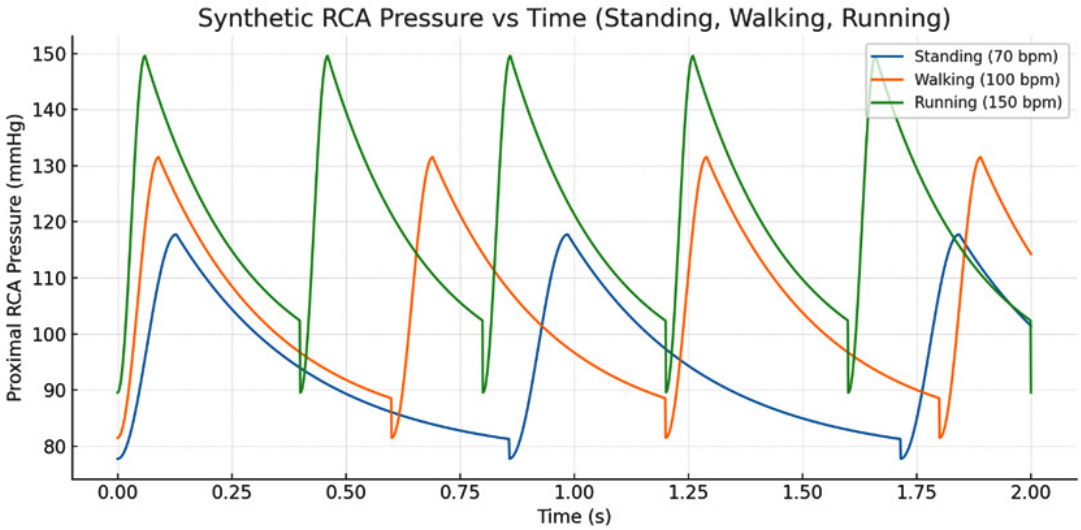

Fig. 3. Synthetic RCA Pressure vs Time under Different Physical Activities

physiologically to increased metabolic demand by amplifies velocity amplitude and decreases cycle time.

Figure 3 shows the change in proximal right coronary artery (RCA) pressure over time scales of standing, walking, and running. In the standing condition (70 bpm), the pressure waveform exhibits systolic ranges of approximately 115-118 mm Hg and diastolic pressure of approximately 78-80 mm Hg, which gives an average pressure of ~95mm Hg. At walking (100 bpm), the shape of the waveform becomes more acute, and systolic

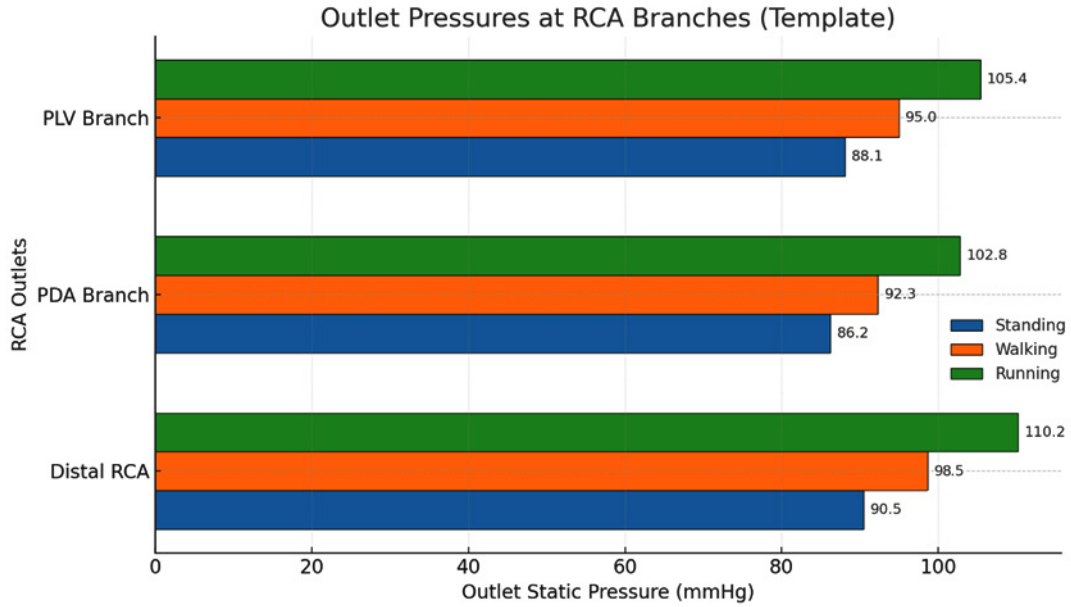

Fig. 4. Outlet Pressures at RCA Branches under Different Physical Activities

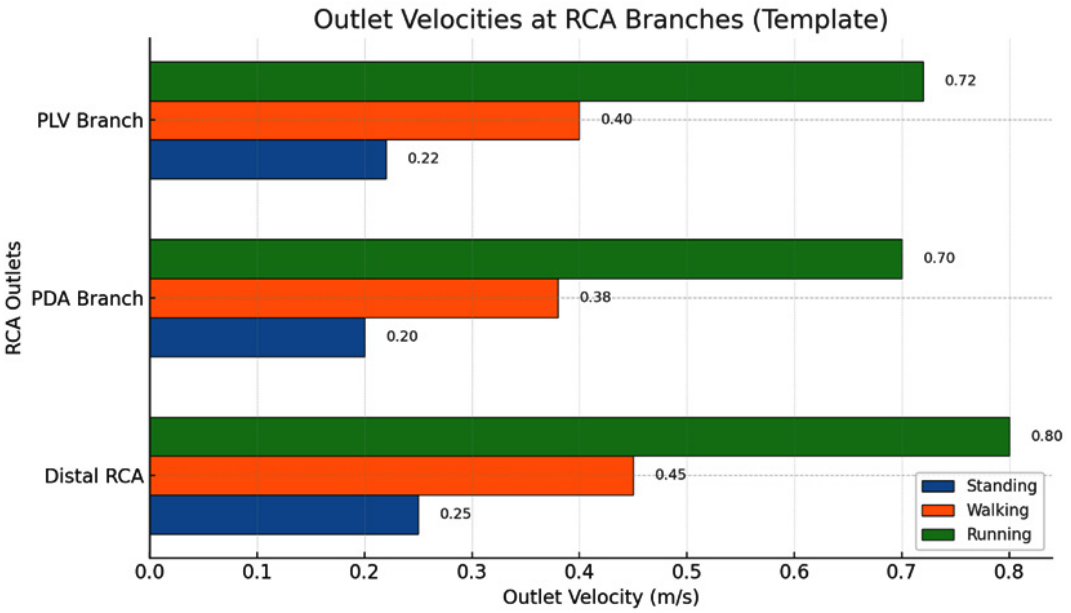

Fig. 5. Outlet Velocities at RCA Branches under Different Physical Activities

peaks are about 130-132 mm Hg, diastolic minima about 82 mm Hg with an increase in the mean up to 105 mm Hg. In the running example (150 bpm), the effect is even greater, With systolic peaks of 148-150 mm Hg and diastolic levels being around 90 mm Hg, the mean value is ~120 mm Hg. The heart cycle reduces in duration to ~0.85 s during rest, ~0.6 s when walking, and ~0.4 s when running providing more frequent variations in pressure. The figure shows the physiological adaptation of the coronary hemodynamics to an increased physical demand where both the systolic pressure and diastolic pressure augment, the pulsation frequency augments noticeably. This is indicative of the increased workload by myocardium and requirement of perfusion during exercise.

Figure 4 shows the outlet static pressures in three branches of the right coronary artery (RCA), i.e. the distal RCA, the posterior descending artery (PDA), and the posterolateral ventricular (PLV) branch, during standing, walking, and running. At rest (standing), the pressures are relatively low

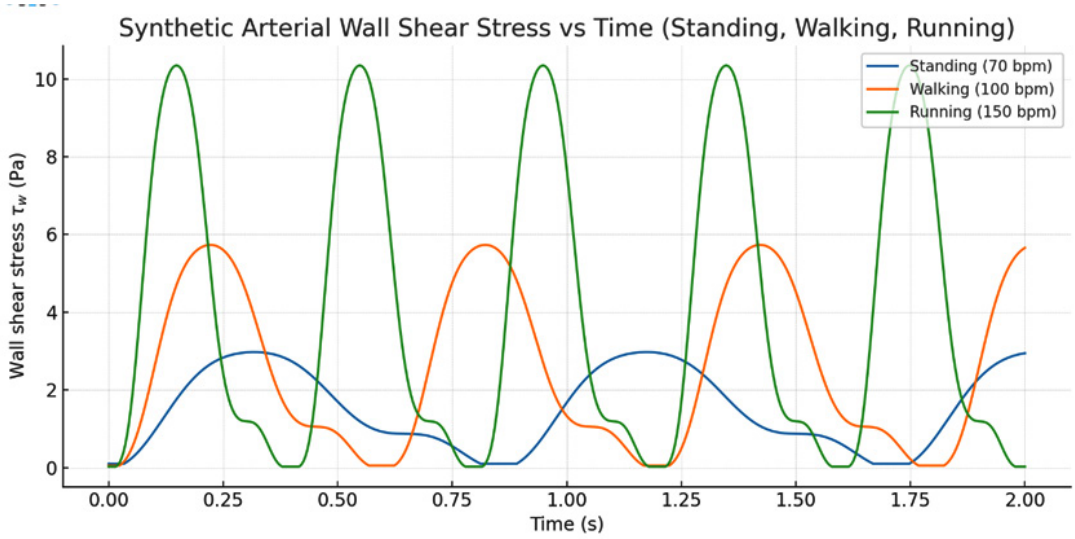

Fig. 6. Arterial Wall Shear Stress vs Time under Different Physical Activities

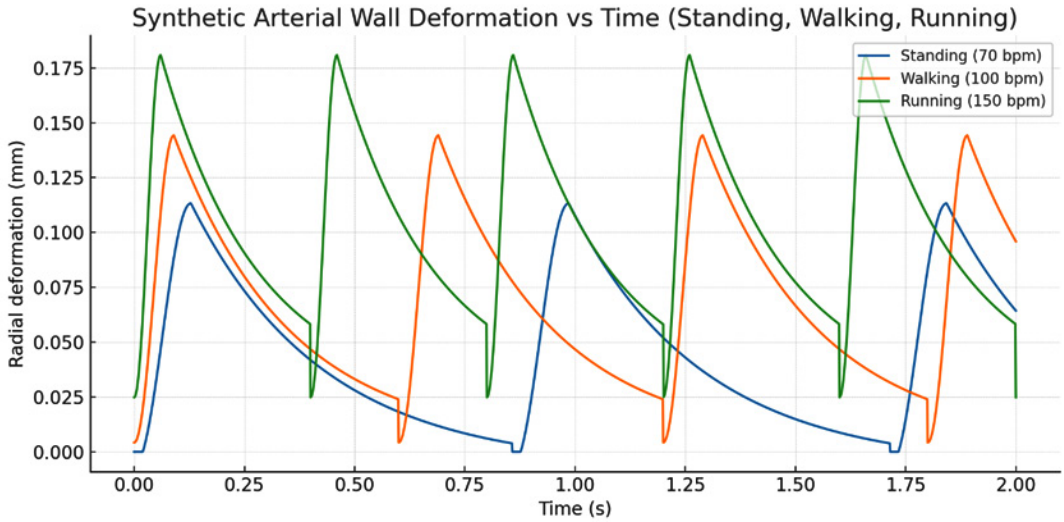

Fig. 7. Arterial Wall Deformation vs Time under Different Physical Activities

with values between 86.2 mm Hg in PDA branch and 90.5 mm Hg in distal RCA and 88.1 mm Hg in PLV branch. There is also a big increase in the outlet pressures with turning to reach 98.7 mm Hg in the distal RCA, 92.3 mm Hg in the PDA, and 95.0 mm Hg in the PLV. When in running conditions, conditions are most pressurized: about 110.2 mm Hg respectively in the distal RCA, 102.8 mm Hg in the PDA, and 105.4 mm Hg in the PLV. The data analysis reveals that there is a continuous increase in outlet pressures as the physical activity increases at all the three branches with the distal RCA having the greatest outlet pressures. This is in the form of physiologic increase in coronary perfusion pressure to account the higher myocardial oxygen demand during exercise.

Figure 5 shows the measures of the outlet blood velocities of three of the branches of the right coronary artery (RCA): distal RCA, posterior descending artery (PDA), posterolateral ventricular (PLV) branches instant during standing, walking, and running. In the standing condition, velocities are lower (by around 0.25 m/s in the distal RCA, 0.20 m/s in the PDA and 0.22 m/s in the PLV branch), due to lower metabolic demand at rest. The outlet velocities nearly doubled when in the walking position and excluding the distal RCA, the values were 0.38 m/s in the PDA and 0.40 m/s in the PLV branch. In running, the velocities turn out to be highest in the distal RCA of 0.80 m/s, followed by the PDA of 0.70 m/s and the PLV branch which is 0.72 m/s. Consistency across the

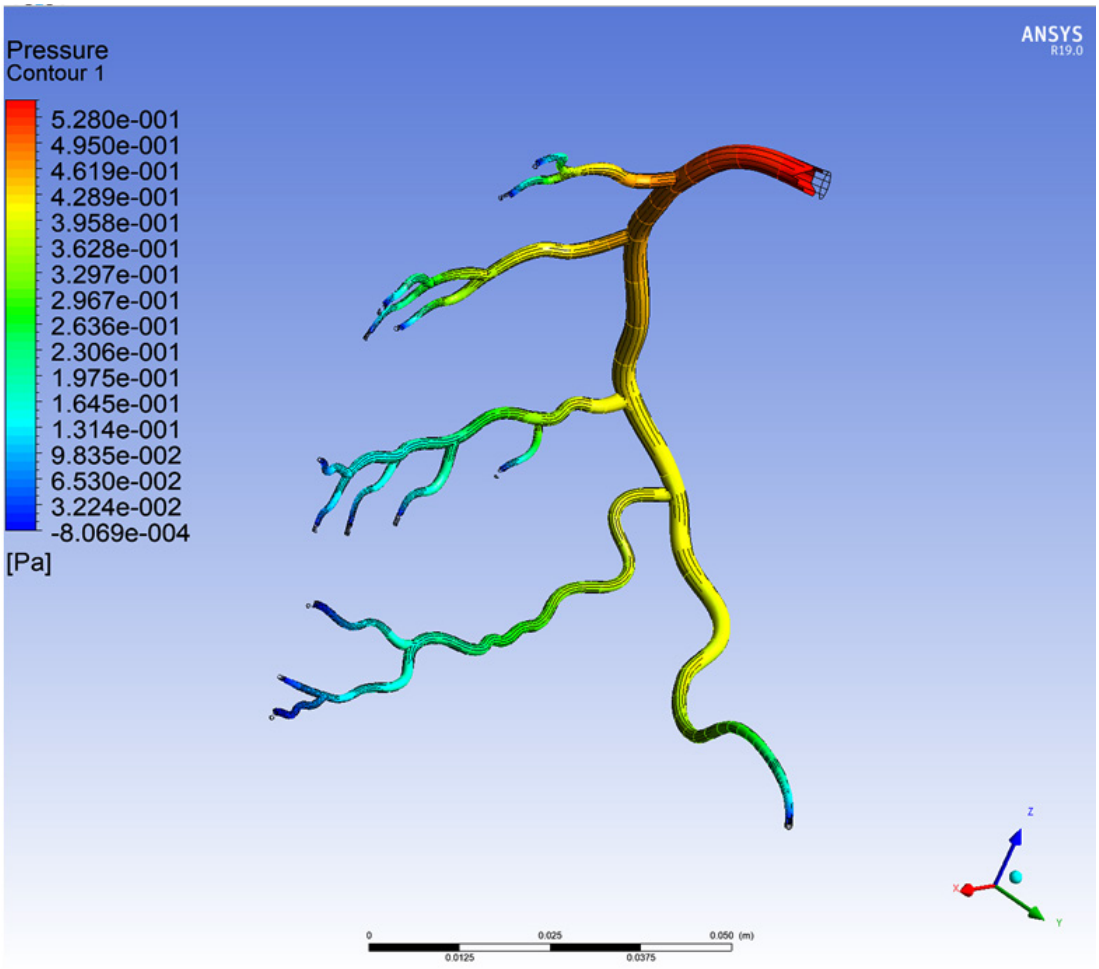

Fig. 8. Pressure Distribution along Coronary Arteries (ANSYS Fluent Simulation)

branches in pointing to a trend of physiological adaptation of the coronary circulation to exercise with increasing cardiac output and coronary flow leading to increasing outlet velocities. The distal RCA has the greatest increase in velocity implying that it is involved in providing greater perfusion to the myocardium in high-activity states.

Figure 6 shows the differences in wall shear stress on the arterial wall understanding, walking, and running. In the standing position (70 bpm), shear stress is relatively small, about 2.8-3.0 Pa maximum and 0-0.5 Pa at baseline, when the demand of coronary flow is low. A significantly sharper waveform with higher peaks of about 5.5 - 5.8 Pa about twice as large as in the standing case and valleys occasionally going to near-zero are observed when ambulating (100 bpm). Moreover, sudden systolic-diastolic swings result in peaks that exceed 10 Pa. At rest, the heart rate is between 60-100 bpm and keeps the cardiac cycle between ~0.85 s, decreasing when walking and running, i.e. ~0.6 and 0.4 s, or more, according to a prevailing opinion, respectively. This shows that there is an increased amplitude and faster oscillations in ôw when the activity level is high.

The radial deformation of the arterial wall as done in standing posture, walking, running, is displayed in Figure 7. When comparing the deformation amplitude of the standing (70 bpm) case, at the peak of ~0.11-0.12 mm, the range of vessel expansion is also minimal. In walking (100 bpm), deformation becomes augmented and peaks occur at around 0.14-0.15 mm, as flow demands measure up to the high systolic blood pressures.

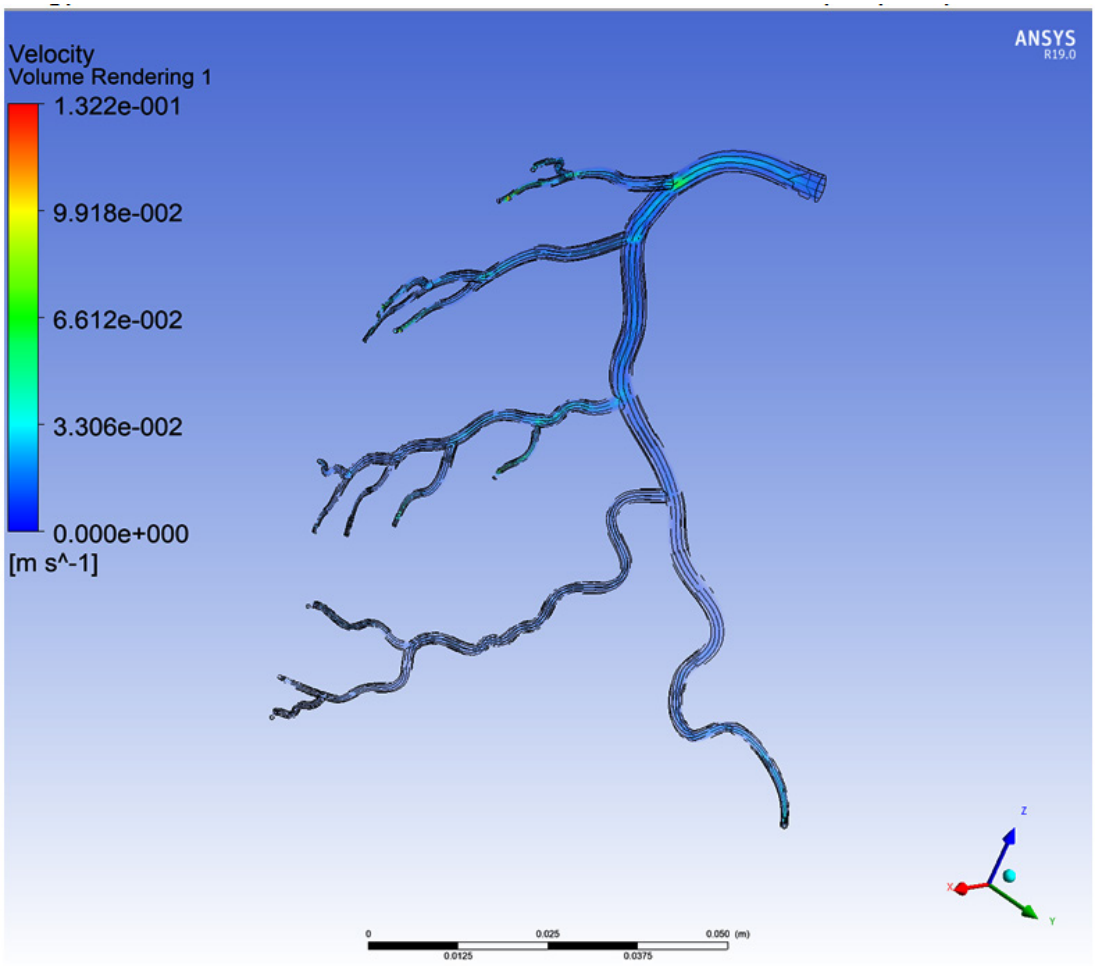

Fig. 9. Velocity Distribution along Coronary Arteries (ANSYS Fluent Simulation)

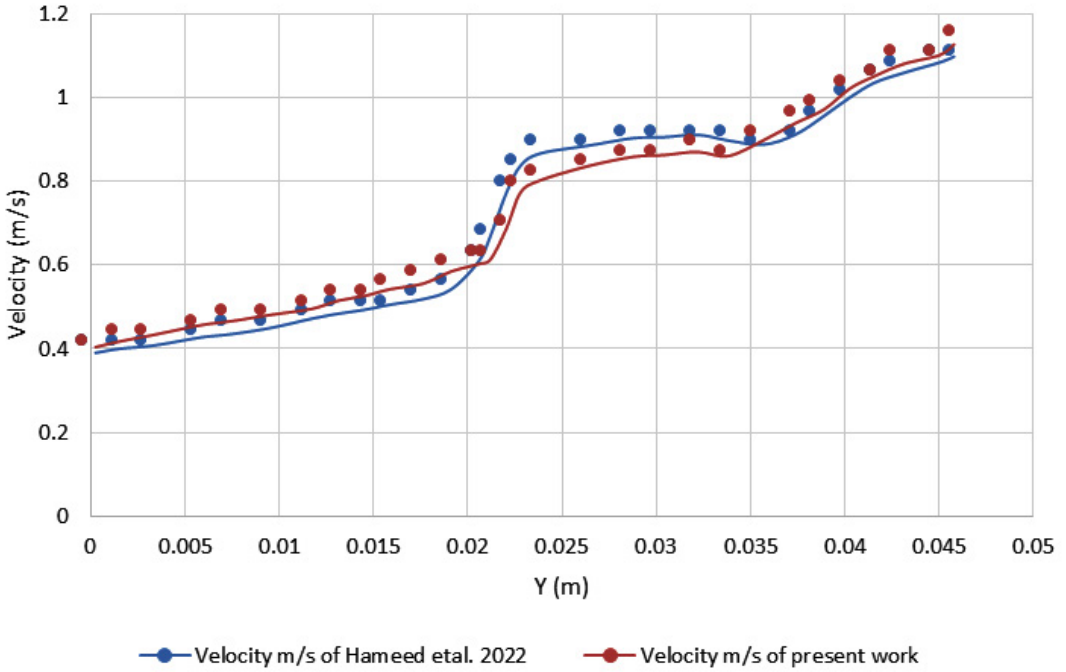

Fig. 10. Velocity variation for stenosed and stented models at near peak systole.

The highest lift can be seen under the running situation (150 bpm), when a sharp cycle peak of about 0.18 mm is on its verge of possibility; it is almost 60 percent improved compared to standing. The rate of beating also increases based on the increase in activity, where the cardiac cycle lasts max ~0.85 s at rest, ~0.6 s during walking and ~0.4 s in running. The between-peaks decay is rapid, closer to baseline, in the same way as the velocity decreases distally due to area expansion in diastole.

Figure 8 demonstrates the pressure-distribution contour on a 3D coronary artery model based on ANSYS Fluent. The region of the main coronary trunk adjacent to the inlet has the maximum pressure, which is about 0.528Pa max as depicted in red. Most of the pressure is lost through viscous forces, and branching as the velocity decreases distally due to area expansionstream into progressively smaller branches. Pressures increase in intermediate parts of arteries (0.25-0.40 Pa; yellow to green), and pressure decay is expected across bifurcations. Blue and dark blue colors represent the lowest pressures appearing at distal branches, in the range of 0.03 Pa and even negative values (not shown) at some outlets. The proximal to distal arterial gradient shown in the graph represents a physiological pressure drawn that preserves the supply of myocardial tissue. The distribution similarly shows the impact of curvature and bifurcation on local hemodynamics, whereby smooth areas have a higher pressure and more pressure is lost down narrow distal blood vessels. In general, the figure illustrates the desirable physiological rate of pressure decrease through the coronary network.

Figure 9 shows the field of velocity distributions within the coronary artery network calculated by ANSYS Fluent. The maximum velocities found in the proximal inlet area record velocities of about 0.132 m/s (red zone). Once velocity decreases distally due to area expansion the major branches, there is a progressive slowdown because of the branching and the increment in the cross-sectional area. Central portions of the branches indicate the velocity between 0.03 m/s-0.10 m/s (green to yellow), due to redistribution of the flow through the bifurcations. Velocities in the distal, narrower branches are slowed further, – to about 0.01 m/s, and some near-wall and outlet areas achieve zero m/s (blue). This velocity degradation represents the physiological adaption of the coronary blood flow where the central

arteries convey blood flows with high momentum that gradually decelerate within the periphery to feed the peripheral myocardium. The distribution also emphasizes the effects of branching angles and the curvature of the vessels that create local velocity differences and therefore are the cause of secondary flows. The figure overall shows the dissipation of the energy of flow in the arterial tree and its effectiveness in the periphery.

The comparison with prior studies (Hameed et al.[27]) confirms the reliability of the present CFD model, as its velocity distribution closely matches published results—with less than 7% deviation—demonstrating that the proposed simulation accurately reproduces realistic post-stenosis hemodynamic behavior.

Figure 10 shows a comparison between the velocity at Y-direction in the current study and the study done by Hameed et al. Both curves have common direction (growing) with the beginning of about 0.4 m/s at Y = 0 m and an increment to 1.1 m/s at Y = 0.045 m. The largest difference lies in the midsection (Y = 0.022-0.030 m), where Hameed et al has a velocity 0.05-0.06 m/s greater, or about 5-7 % of the difference. Beyond this region, there is indeed convergence of the results with a difference of less than 2% at the inlet and outlet ends. In general, the model used in the current study proves to be reliable as it is validated successfully with the reference one.

The comparison of the performance of the current simulation to Hameed et al. (2022) also yields a strong quantitative agreement (Fig. 10). Both velocity profiles generally have essentially the same Y-axis trend with maximum deviation 5–7% for mid-section and convergence to be observed at the inlet and outlet. This strong correlation also evidences solid numerical accuracy and robustness of the CFD model in operation as well as validates the ability of CFD model to consistently capture the post-stenotic flow dynamics and mimic the realistic hemodynamics experienced in earlier experimental and numerical investigations.

DISCUSSION

The numerical simulations provided a thorough biomechanical characterization of pulsatile blood flow for a stenosed RCA at three physiological states: standing (rest), walking (moderate exercise), and running (vigorous activity). The results revealed a steady rise in hemodynamic loads with increasing activity, highlighting the adaptability of coronary circulation and the added biomechanical stresses that may accelerate coronary artery disease progression. Changes of blood flow velocities during exercise are more pronounced than in between states. Blood flow velocity increased notably from rest to walking and running, reflecting the heart's adaptive response to higher metabolic demand and demonstrating how exercise amplifies coronary flow dynamics under progressive workloads. This increase is related to the higher cardiac output and the higher oxygen requirements produced during exercise. A redistribution of velocity at bifurcations also underlined the importance of branching geometry in influencing the local hemodynamics. Coronary pressure showed a comparable profile: mean pressures increased from ~95 mm Hg at rest to ~105 mm Hg during walking, and reached ~120 mm Hg during running. The outlet pressures across RCA branches (distal RCA, PDA, PLV) were steadily increasing with activity, but highest rise was observed with distal RCA. The physiological effect of increased perfusion pressure on myocardial oxygen supply during workloads is further supported with the findings described here, although stenotic regions experience elevated mechanical loading under higher workloads. WSS analysis offered important information on endothelial loading. At rest, WSS averaged 2.8–3.0 Pa, increased to 5.5–5.8 Pa during walking, and >10 Pa in running. WSS oscillated more with activity-induced increase in WSS, with more pronounced systolic-diastolic changes at higher activity. These oscillatory properties are clinically useful as acute changes in WSS relate to endothelial dysfunction, plaque failure and progress of stenosis. Part of the simulations, Fluid–Structure Interaction (FSI), showed that arterial compliance was higher under pulsatile loading. Radial deformation was lowest for rest (0.11–0.12 mm), moderate for walking (0.14–0.15 mm), and peaked for running (0.18 mm), nearly 60% increase relative to rest. The increased frequency and amplitude of deformation under exercise reflect mechanical pressure on the arterial walls, an important factor known to contribute to plaque rupture risk. When combined, the findings indicate that exercise causes non-linear increases

in velocity, pressure, WSS, and wall deformation. When a vessel is stenosed, including the RCA, these physiological adaptations are beneficial, but may also lead to increased biomechanics and thus accelerated disease progression. Specifically elevated WSS and cyclic wall strain upon running indicate an elevated risk of endothelium injury and plaque instability. The results indicate that moderate exercise improves efficiency of coronary flow through physiological adaptation, whereas high-intensity exercise puts significant hemodynamic and mechanical burdens on vascular structures potentially challenging vascular integrity in stenosed arteries. These conclusions support the need to specify safe exercise thresholds for patients with coronary disease. The overall CFD and FSI analyses thereby contribute quantitative insight for personalized diagnosis, therapeutic planning, and exercise prescription, stressing the balance between beneficial adaptation and excessive vascular stress.

CONCLUSION

This paper used Computational Fluid Dynamics (CFD) and fluid-structure interaction (FSI) to simulate the biomechanical behavior of a pulsatile blood flow in a stenosed Right Coronary Artery (RCA) in three different physical states, namely, standing (rest), walking (moderate activity) and running (vigorous activity). Individualized three-dimensional arterial geometry and pulsatile inlet boundary were used to assess important hemodynamic parameters such as velocity, pressure, wall shear stress (WSS), and arterial deformation of the walls. The results of simulations shown explain the impact that changes in physical activity have on vasculature hemodynamics and vessel wall reaction directly.

When resting (70 bpm), blood velocity was low (0.20–0.50 m/s, arterial pressure ~ 95 mm Hg). Outlet velocities ranged from 0.20–0.25 m/s, the average wall shear stress (WSS) was 2.8–3.0 Pa, and arterial wall deformation was 0.11–0.12 mm. However, during moderate activity (walking, 100 bpm), the velocity increased to almost double to ~1.1 m/s and the mean pressure increased to 105 mm Hg. Outlet velocities climbed up to 0.38–0.45 m/s, WSS increased to 5.5–5.8 Pa and wall deformation grew to 0.14–0.15 mm, corresponding to higher mechanical loading. At vigorous activity (running at 150 bpm), velocity was maximum at 2.2–2.3 m/s, which is about four times higher than at rest, mean pressure was 120 mm Hg, and outlet velocities were 0.70–0.80 m/s, the corresponding WSS exceeded 10 Pa and wall deformation reached 0.18 mm, and the increase of approximately 60 % compared to walking condition.

ACKNOWLEDGEMENT

The author would like to thank Anatomy Department, College of Medicine, University of Baghdad, Iraq for their guidance during the work.

Funding Sources

The author(s) received no financial support for the research, authorship, and/or publication of this article.

Conflict of Interest

The author(s) do not have any conflict of interest.

Data Availability Statement

This statement does not apply to this article.

Ethics Statement

This research did not involve human participants, animal subjects, or any material that requires ethical approval.

Informed Consent Statement

This study did not involve human participants, and therefore, informed consent was not required.

Clinical Trial Registration

This research does not involve any clinical trials.

Permission to reproduce material from other sources

Not Applicable

Author Contributions

The sole author was responsible for the conceptualization, methodology, data collection, analysis, writing, and final approval of the manuscript

REFERENCES

1. Freidoonimehr N, Ahmadian MT, Zamani R. A numerical study of fluid–structure interaction in a stenosed coronary artery with different plaque compositions. *J Appl Comput Mech*. 2020;6(2):264–274. https://doi.org/10.22055/JACM.2019.29421.1699

2. Gholipour A, Shariati M, Toghraie D. Computational modeling of pulsatile blood flow in stenotic arteries considering non-Newtonian behavior. *Comput Biol Med*. 2018;103:34–43. https://doi.org/10.1016/j.compbiomed.2018.10.006
3. He X, Ku DN. Pulsatile flow in the human left coronary artery bifurcation: Average conditions. *J Biomech Eng*. 1996;118(1):74–82. https://doi.org/10.1115/1.2795949
4. Alizadeh M, Firoozabadi B, Shahmardan M. Numerical simulation of pulsatile blood flow in a realistic stenosed artery considering non-Newtonian models. *Biomed Eng Comput Biol*. 2014;6:1–9. https://doi.org/10.4137/BECB.S13234
5. Bani-Hani R, Abu Al-Rub RK, Abdel-Wahab AA. A biomechanical approach for the study of blood flow and wall stress in stenosed arteries under pulsatile conditions. *Biomed Eng Appl Basis Commun*. 2015;27(4):1550030. https://doi.org/10.4015/S1016237215500302
6. Back LH, Kwack EY, Back MR, Crawford DW. Flow dynamics in curved and bifurcating arteries with stenosis: A review. *J Biomech*. 1977;10(10):759–768.
7. Beier S, Ormiston J, Webster M, Cater J, Norris R. A patient-specific CFD model of coronary artery blood flow: Validation and application to exercise. *Ann Biomed Eng*. 2016;44(9):2783–2795. https://doi.org/10.1007/s10439-016-1594-2
8. Belzacq AS, Prevost R, Fontaine J. CFD-based physiological modeling of coronary perfusion under stress conditions. *Comput Biol Med*. 2012;42(3):318–326. https://doi.org/10.1016/j.compbiomed.2011.12.003
9. Eberth JF. Biomechanical Stimuli in Vascular Remodeling: A Study Using Murine Models and Computational Simulation [dissertation]. *College Station (TX): Texas A&M University*; 2008. Available from: https://oaktrust.library.tamu.edu/handle/1969.1/ETD-TAMU-2661
10. Pandey A, Dubey RK, Srivastava S. CFD analysis of pulsatile flow in a left coronary artery with different levels of stenosis. *Numer Heat Transf Part A Appl*. 2020;78(11):1043–1058. https://doi.org/10.1080/10407782.2020.1767167
11. Piskin S, Celebi MS. Effects of different inlet velocity profiles on hemodynamic parameters of the patient-specific carotid artery bifurcation: A CFD study. *Comput Biol Med*. 2013;43(6):717–728. https://doi.org/10.1016/j.compbiomed.2013.03.006
12. Kouhi A, Kermani MJ, Farahani MM. Investigation of the blood flow in curved artery using fluid–structure interaction. *Kowsar Med J*. 2008;13(2):85–92.
13. Li Z, Kleinstreuer C, Archie JP. Hemodynamic factors and atherogenesis in a human abdominal aorta bifurcation model. *Med Eng Phys*. 2007;29(8):877–884. https://doi.org/10.1016/j.medengphy.2006.09.007
14. Liu X, Fan Y, Deng X, Zhan F. Effect of non-Newtonian and pulsatile blood flow on hemodynamics in a stenosed artery. *J Biomech*. 2012;45(2):362–369. https://doi.org/10.1016/j.jbiomech.2011.10.024
15. McCallinhart PE, Lorthois S, Guibert R. Coronary remodeling and biomechanics: Are we going with the flow in 2020? *Front Physiol*. 2021;12:645736. https://doi.org/10.3389/fphys.2021.645736
16. Moore JE, Ethier CR. Computational modeling of blood flow and atherosclerosis. *Front Biosci (Elite Ed)*. 2010;2:919–937. https://doi.org/10.2741/e130
17. Jung J, Lyczkowski RW, Panchal CB, Hassanein A. Multiphase CFD modeling of pulsatile blood flow in a bifurcating artery. *Korean Circ J*. 2006;36(10):881–887. https://doi.org/10.4070/kcj.2006.36.10.881
18. Pivkin IV, Richardson PD, Karniadakis GE. Blood flow velocity effects and role of activation delay time on growth and form of platelet thrombi. *Proc Natl Acad Sci U S A*. 2005;103(46):17164–17169. https://doi.org/10.1073/pnas.0607949103
19. Qiu Y, Tarbell JM. Numerical simulation of pulsatile flow in a compliant tapered carotid bifurcation model. *J Biomech Eng*. 1999;121(1):77–83. https://doi.org/10.1115/1.2834964
20. Razavi A, Shirani E, Sadeghi MR. Numerical simulation of blood pulsatile flow in a stenosed carotid artery using different turbulence models. *J Biomech*. 2011;44(11):2021–2030. https://doi.org/10.1016/j.jbiomech.2011.04.010
21. Saeidkhalafvand S, Bozorgzadeh B, Hassani K. Numerical simulation of blood flow through a realistic human aortic arch under different cardiac cycle modes. *Comput Methods Biomech Biomed Engin*. 2015;18(2):149–157. https://doi.org/10.1080/10255842.2013.779682
22. Stroud JS, Berger SA, Saloner D, Reddy V. Influence of stenosis morphology on flow through severely stenotic vessels: Implications for plaque rupture. *J Biomech*. 2001;33(4):443–455. https://doi.org/10.1016/S0021-9290(99)00189-6
23. Wong GCK, How TV, Wheatley DJ. Numerical simulation of flow dynamics in a realistic aortic arch geometry using computational fluid dynamics. *J Med Biol Eng*. 2013;33(2):188–195. https://doi.org/10.5405/jmbe.1225

24. Wu W, Jin Z, Fisher J. Influence of dynamic loads on the wear of hip implants. Wear. 2014;311(1–2):210–217. https://doi.org/10.1016/j.wear.2013.12.001
25. Younis HF, Kaazempur-Mofrad MR, Chan RC, et al. Hemodynamics and wall mechanics in human carotid bifurcation and its consequences for atherogenesis: Investigation of inter-individual variation. *Biomech Model Mechanobiol*. 2004;3(1):17–32. https://doi.org/10.1007/s10237-004-0042-2
26. Zendehbudi A, Arzani A. Simulation of flow in a stenosed artery using a three-dimensional model. *Math Comput Model*. 1999;30(3–4):83–94. https://doi.org/10.1016/S0895-7177(99)00140-2
27. Vemavarapu S, Panigrahi BK. Comparison of blood flow analysis in stenosed and stented carotid artery bifurcation models. *J Braz Soc Mech Sci Eng*. 2021;43(5):1–12. https://doi.org/10.1007/s40430-021-02917-4